Membrane rupture and independent extension of sister membranes drive cytokinesis in *C. elegans* embryos

Jingjing Liang[1]*, Tingrui Huang[1,2,3], Xun Huang[1,2], and Mei Ding[1,2]*

[1] Institute of Genetics and Developmental Biology, Chinese Academy of Sciences, Beijing 100101, China

[2] Taikang Center for Life and Medical Sciences, School of Basic Medical Sciences, Wuhan University, Wuhan 430071, China

[3] University of Chinese Academy of Sciences, Beijing 100049, China

* Correspondence: jjliang@genetics.ac.cn; mding@genetics.ac.cn

Abstract

Cell division, the physical separation of a cell into two daughter cells, is classically thought to require continuous plasma membrane invagination driven by equatorial contractile forces. Here, we challenge this paradigm by uncovering an unexpected mechanism in *C. elegans* embryos: the plasma membrane ruptures as early as metaphase. Instead of invaginating as a continuous sheet, the separated membranes extend independently to partition the cytoplasm. The membrane rupture and independent extension of sister membranes create membrane discontinuities—widely observed in electron microscopy (EM) sections. Without plasma membrane coverage, the exposed cytoplasmic regions are shielded either by plasma membrane from neighboring, likely kinship, cells or extracellular matrix components, preventing massive leakage. Our findings overturn the long-standing assumption that cytokinesis requires persistent membrane integrity, and offer fresh insights into cell division, particularly in fast dividing embryonic cells.

Introduction

The plasma membrane integrity is the corner stone of cell biology. Based upon, , current models further propose that cell division should also occur with uninterrupted membrane integrity and the invagination of this intact membrane, driven by a contractile ring of actin filaments, myosin II, and regulatory proteins (Pollard and O'Shaughnessy, 2019), with vesicle fusion supplying new membrane to accommodate shape change (Gerien and Wu, 2018), progressively deepens until pinching the cell into two daughter cells (Figure 1A). Critically, the foundational premise of uninterrupted membrane integrity during cytokinesis has never been rigorously tested until our unexpected discovery in *C. elegans* embryos.

After fertilization, the single cell *C. elegans* embryo begins a series of highly stereotyped cell divisions. During this phase, cells undergo rapid division (15-30 minutes per cycle), with each cycle alternating between S (DNA synthesis) and M (mitosis and cytokinesis) phases while bypassing G1and G2 gap phases until the 28-cell stage (Edgar and McGhee, 1988; Deppe et al., 1978; Sulston et al., 1983; Bao et al., 2008; Pintard and Bowerman, 2019). Around this stage, the worm embryos are laid by the mother. Subsequent development continues outside the mother, encapsulated within a protective, multi-layer extracellular matrix known as the eggshell (Stein, 2018). This impermeable eggshell is established earlier, by the end of anaphase II of meiosis, and undergoes its final modifications during the embryo's first few mitotic divisions (Bembenek et al., 2007; Zhang et al., 2005).

During routine ultrastructural analysis (Zhu et al., 2022), we found that rather than maintaining membrane continuity, the dividing *C. elegans* embryonic cells routinely exhibit plasma membrane discontinuities. Further analysis revealed that the

plasma membrane of the embryonic cells ruptures as early as metaphase and sister membrane primarily extend independent from each other to achieve cytoplasmic partition (Figure 1B), a mechanism never before documented. This discovery challenges the canonical view of cytokinesis at its core, revealing an unanticipated plasticity in cell division mechanisms and prompting a re-evaluation of how membrane dynamics are regulated across species.

Results

Widespread membrane discontinuities in dividing *C. elegans* embryonic cells

Our study was initially prompted by the curious observation that the plasma membrane of embryonic cells in *C. elegans* does not appear to be continuously intact. We refer to these membrane discontinuities as membrane openings (MOs). They are particularly evident at the embryo's periphery. As shown in Figure 1C, the plasma membrane is absent in the region marked by the white dashed line. Membrane interruptions are also be observed in the embryo's central regions. For instance, Figure 1D shows that Cell 3 contains a MO facing both Cell 1 and Cell 2. Additionally, we noted instances where a single plasma membrane (SPM) appears to traverse the cytoplasm, seemingly partitioning it into separate compartments across adjacent cells (Figure 1D) (yellow arrows). According to the conventional view, the plasma membrane should remain intact throughout the cell cycle—whether during division or interphase—and each cell should be enclosed by its own membrane. Consequently, between two adjacent cells, we would expect to observe two distinct plasma membranes. The presence of a single continuous membrane, however, suggests the existence of regions lacking a complete boundary. For instance, Cell 4 in Figure 1D clearly contains such membrane discontinuities. Collectively, these

74 findings challenge the established notion that the plasma membrane remains intact
75 over the entire lifetime of a cell.

76 To rule out potential artifacts inherent to electron microscopy (EM) techniques,
77 we performed a series of control experiments. First, we prepared four independent
78 sample batches. Membrane discontinuities were consistently observed in all batches,
79 indicating that the phenomenon is not specific to a single preparation. Second, we
80 examined a publicly available historical collection of *C. elegans* embryo EM images
81 (Wormatlas) and identified MOs in several instances, particularly at the embryonic
82 periphery. This confirmation in an independent dataset suggests that MOs are genuine
83 cellular structures rather than procedural artifacts. Third, we analyzed embryos across
84 various developmental stages. MO-containing cells were observed in both intrauterine
85 and already laid embryos at early stages (Figure S1). However, as embryos reached
86 the comma stage (Figure S2)—a period characterized by the onset of elongation and a
87 decline in active cell proliferation—the incidence of MOs dropped dramatically
88 (observed in 0/13, 0/17, 0/30, and 0/30 cells examined, respectively). These results
89 demonstrate that plasma membrane discontinuities are associated with specific stages
90 of *C. elegans* embryogenesis and are not a product of random membrane tearing.

91 The early stage of *C. elegans* embryonic cells is under rapid and extensive cell
92 division. Within approximately 100 minutes, a two-cell embryo develops into an
93 embryo containing nearly 30 cells (Bao et al., 2008). Given this dynamic
94 proliferation, we suspected that the formation of membrane discontinuities might be
95 associated with cell division events. Therefore, to systematically examine the
96 formation of membrane discontinuities, we collected EM images of 60 early embryos
97 from 9 gravid adults. By examining the entire circumference of 425 cells in single

98 high-pressure freezing transmission electron microscopy (HPF-TEM) sections (Figure
99 S2) (Modern Electron Microscopy Methods for C. elegans, 2012), we found that MOs
100 in 159 cells distributed across 57 embryos, representing 95% of the total sampled
101 embryos (Figure 1E). Among these 159 affected cells, 89% (141/159) exhibited a
102 single membrane discontinuity, while 13 cells had two openings and 5 cells had three.

103 We analyzed the 159 cells exhibiting MOs based on nuclear and cytoplasmic
104 morphology (Figure 1E). Of these, 64 cells appeared in EM sections containing only
105 cytoplasmic regions—9 of which completely lacked discernible plasma membranes.
106 The remaining 95 cells contained one or more nuclei or condensed chromosomes.
107 Among them, 10 cells were clearly in metaphase stage (defined by a single
108 chromosomal cluster). As shown in Figure 2A, a representative metaphase cell (MC)
109 displayed a MO (dashed white line) spanning roughly one-third of the cell's
110 circumference. High-magnification imaging revealed that in contrast to the wrinkled
111 plasma membranes (Figure 2A, enlarged boxed area displayed in 1), the large MO
112 exhibited a smoother surface morphology, and the internal cytoplasm remained
113 enclosed within the cell (Figure 2A, enlarged boxed areas displayed in 2 and 3). MOs
114 were also observed in anaphase cells (AC) (n=5; characterized by <10 chromosomal
115 clumps; Figure 2B, enlarged in 2) and telophase cells (n=5; defined by two nuclei
116 sharing cytoplasm). Intriguingly, one telophase-like cell contained three nuclei within
117 a common cytoplasm (Figure S2, marked by &).

118 Because EM sectioning captures cells at random stages of the cell cycle, we
119 sought to systematically assess the relationship between mitosis and MOs. To do so,
120 we analyzed 20 cells with unambiguous division features, selected based on nuclear
121 morphology—such as aligned chromosomes (metaphase) or discrete clusters

122 (anaphase)—and cytoplasmic sharing, indicated by two or more nuclei within a
123 common cytoplasm (telophase). Strikingly, 19 out of 20 cells (95%) revealed MOs
124 upon tracing the plasma membrane in single EM sections (Figure S3). This near-
125 ubiquitous association strongly suggests that membrane discontinuities are an integral
126 feature of cell division in early *C. elegans* embryos.

127 **Membrane rupture in cells at metaphase**

128 The observed membrane discontinuities suggest that the plasma membrane of early *C.*
129 *elegans* embryos may rupture during cell division. However, because TEM provides
130 only static, two-dimensional images, we could not determine the three-dimensional
131 nature of these ruptures. To better understand this phenomenon, we acquired
132 continuous serial sections and performed 3D reconstruction.

133 Since membrane discontinuities appear at metaphase—well before nuclear or
134 cytoplasmic division—we performed continuous EM sectioning to trace the entire
135 plasma membrane of a metaphase cell (Figures 2C). Through 3D reconstruction, we
136 identified a continuous plasma membrane rupture extending over 8,940 nm, which is
137 more than two-thirds of the cell's circumference (Figure 2D). Notably, one end of the
138 membrane rupture appeared long and narrow, while the other was wide and exhibited
139 cytoplasmic leakage (Figure 2D and Video S1). Further analysis revealed that the
140 leaked cytoplasm remained confined to a relatively localized region (Video S1).
141 During metaphase, chromosomes align at the equatorial plane, a key region for
142 subsequent segregation. To explore the spatial relationship between membrane
143 rupture and chromosomal organization, we further reconstructed the entire condensed
144 chromosome region (Figures 2C). We found that this large-scale membrane rupture

145 largely encircled the chromosomal disc (Figure 2D and Video S1), spatially aligning
146 with the future segregation zone.

147 **The detachment of sister membranes**

148 According to the conventional model, cytokinesis in animal cells begins with the
149 formation of a membrane invagination. As this invagination deepens, it gives rise to
150 two back-to-back membrane layers, ultimately leading to the physical separation of
151 the two daughter cells. In the context of membrane rupture, however, plasma
152 membrane disruption results in the separation of two putative sister membranes. We
153 then asked how the subsequent cytokinesis process proceeds with detached sister
154 membranes. To address this question, we examined 51 dividing cells. In each of these
155 cells, two well-separated nuclei were observed, indicating that they were at telophase.
156 We found that while a minority of cells (6/51) exhibited classical membrane
157 invagination (Figure 3A), including one embryo transitioning from the one-cell to the
158 two-cell stage, the vast majority (45/51) displayed a striking detached membrane
159 configuration (Figure 3B). In these cases, sister membrane tips were completely
160 separated from each other (Figures 3B and 3C, marked with *), forming distinct, non-
161 contiguous structures that defy conventional models of cytokinesis. This predominant
162 pattern suggests that membrane detachment—rather than continuous invagination—
163 may represent the primary mode of cytoplasmic separation in *C. elegans* embryos. Of
164 note, the membrane rupture simultaneously generates individual sister membranes
165 with severed edges. Indeed, as shown in Figure 3B, the tips of both free-ended edges
166 (*) of Cell 1 are visible in the EM section.

167 In the detached membrane configuration, cytoplasmic components—such as
168 glycogen granules and ribosomal particles—were clearly visible surrounding the

169 severed edges of the two sister membranes (Figure 3C). This observation is
170 particularly significant because the classical invagination model cannot generate
171 single plasma membrane barriers between adjacent cytoplasmic domains. Instead,
172 independent extension of severed sister membranes could explain the formation of
173 cytoplasm-immersed membranes. To further test this hypothesis, we traced 12
174 cytoplasm-embedded membranes, including those separating Cell 1 from Cells 2 and
175 3, and those separating Cell 4 from 3 (displayed on Figure 3D, enlarged in 1 and 2). In
176 all cases, the cytoplasmic regions flanking these membranes belonged to cytosolically
177 interconnected sister cells. Together, these results demonstrate that *C. elegans*
178 embryonic cytokinesis relies on detached sister membrane extension rather than
179 invagination mediated by intact membranes.

180 Tracing from the severed edges back to their origins, we found that the sister
181 membranes were frequently anchored side-by-side near the cytosol-immersed region
182 (Figures 4A-4D). Within this region, gap junction plaques were often observed (57 in
183 94 cases) at membrane contact sites (Figure 4B), though their potential role in sister
184 membrane cohesion is unclear. These contact sites alternated with regions where the
185 two sister membranes separated, revealing lightly stained intercellular spaces in EM
186 images. Beyond the anchored region, the separation between sister membranes
187 became evident and each membrane exhibited the characteristic features of a typical
188 plasma membrane—with one side facing the cytosol and the other exposed to the
189 extracellular environment (Figure 4D).

190 Cellular vesicles were observed near free membrane edges (Figures 4A-4C).
191 Some cytosol-immersed membrane tips appeared connected to vesicles (Figure 4A),
192 with instances of direct contact (Figure 4B) and possible fusion events (Figures 4B

193 and 4C). Vesicles also clustered along the anchoring area, as well as the separated
194 sister plasma membranes (Figure 4D). EM analysis revealed no morphological
195 differences between vesicles associated with the cytosol-immersed region and those
196 near conventional regions of the sister membranes (Figures 4B and 4D).

197 **Analysis of a tri-nucleated cell during cytokinesis**

198 To gain more comprehensive insight into membrane organization during cytokinesis,
199 we further applied the AutoCUTS-SEM (automatic collector of ultrathin sections
200 scanning electron microscopy) workflow (Li et al., 2017) to acquire serial EM
201 sections of a telophase cell. Through continuous tracing, we discovered that this cell
202 actually contained three independent nuclei. We color-coded each membrane region
203 according to its associated nucleus, with relative sizes estimated from EM sections to
204 ensure proportional representation (Figure 5A). The 3D model demonstrated that the
205 division plane between the yellow and blue cells was roughly perpendicular to that
206 between the purple cell and the other two (Figure 5A). The presence of three nuclei
207 within a shared cytoplasm suggests that one of the daughter cells entered the next
208 round of cell division without completing the previous one. This phenomenon—
209 concurrent divisions—appears to be common in early *C. elegans* embryos, as our EM
210 analysis identified more than 10 cells with three or four nuclei. For example, Figure
211 3D shows an EM section of a cell containing four nuclei.

212 Using consecutive EM sections, we traced membrane integrity in this tri-
213 nucleated cell. We found that this tri-nucleated cell was enveloped by three distinct
214 plasma membranes, each containing a single rupture site. These three ruptures
215 converged to form a "Y"-shaped exposed cytoplasmic region spanning >351 sections
216 (21,060 nm; Figures 5A and 5B and Video S2). Throughout these 351 consecutive

217 sections, we detected no continuity between adjacent membranes, indicating that
218 membrane independence had been established by this stage. Consecutive tracing
219 further showed that the MOs—frequently observed in single EM sections (Figures 1
220 and 2)—could arise from either the separation between sister membranes (Figure 5C)
221 or from separated edges of the plasma membrane within the same cell (Figure 5D).
222 Additionally, multiple openings within a single cell might represent different cross-
223 sectional planes of a common membrane rupture (Figure 5E).

224 In all three cells (where cytoplasmic separation was incomplete), the free
225 membrane edges were in close proximity (marked by *; Figures 5F and 5G),
226 suggesting they were in late cytokinesis and that membrane extension mediated by
227 detached membranes could persist into this stage. Taken together, these findings
228 demonstrate that this tri-nucleated cell was undergoing concurrent cytokinesis, with
229 three detached membranes independently extending toward a common cytoplasmic
230 region to achieve cytoplasm individualization (Figure 5H). A similar mechanism may
231 operate in four-nucleated cells (Figure 3D, for instance), in which two detached
232 daughter membranes—without completing the last round of cell division—undergo
233 further rupture, forming four granddaughter membranes. These membranes then
234 extend independently to complete cell division (Figure 5H).

235 **Capturing the membrane rupture and independent extension of detached sister**
236 **membranes in living embryos**

237 While high resolution HPF-TEM analysis revealed widespread membrane
238 discontinuities in early *C. elegans* embryos, this static imaging approach cannot
239 capture dynamic membrane behavior. To investigate whether optical microscopy can
240 visualize membrane ruptures and the movement of severed sister membranes, we

241 employed a fluorescence-labeled membrane marker, GFP::PH(PLC1δ1) (see Methods
242 and Materials for details). Our live imaging detected both putative membrane ruptures
243 (Figure 6A) and free-ended sister membrane structures (Figures 6B and 6C),
244 providing additional evidence that membrane rupture and independent extension of
245 detached sister membranes underlie cytokinesis in *C. elegans* embryos (see
246 Discussion).

247 **Sealing the exposed cytosol by neighboring membranes and extracellular matrix**
248 **layers**

249 The integrity of the plasma membrane is essential for cell survival, as its disruption
250 can lead to cytoplasmic leakage and, if severe, result in cell death. However,
251 widespread cytoplasmic leakage has not been observed in wild-type *C.*
252 *elegans* embryos. Based on our EM observations, we propose two mechanisms
253 through which dividing embryonic cells may seal or cover exposed cytosolic regions.

254 First, the sharing of plasma membrane with neighboring cells may protect the
255 exposed cytosol. As repeatedly shown in EM images in this study (Figures 1, 3 and 4),
256 a single elongated free-ended membrane from one cell consistently helps define
257 boundaries with adjacent cells. These neighboring cells may be direct sister cells
258 derived from the same mother cell, or cousin cells originating from mother cells that
259 were once sisters. In cases where three nuclei share a common cytosol, the adjacent
260 cell could even be an aunt or nephew cell.

261 In addition, eggshell components may seal cytoplasmic regions lacking
262 membrane coverage. The *C. elegans* eggshell is composed of six distinct extracellular
263 matrix layers (Olson et al., 2012; Benenati et al., 2009; Rappleye et al., 1999;

264 Schierenberg and Junkersdorf, 1992; Stein, 2018). Among these, the fifth
265 permeability barrier layer (PBL), a lipid-rich structure, serves as the osmotic and
266 permeability barrier for the developing embryo (Olson et al., 2012; Benenati et al.,
267 2009). Normally, the PBL encloses the peri-embryonic layer (PEL), which separates it
268 from the embryonic plasma membrane (Olson et al., 2012; Benenati et al., 2009)
269 (Figures 7A and 7B). In contrast, in regions where the plasma membrane was absent,
270 we observed the PBL adhering directly to the exposed cytoplasm (red triangles and
271 dashed red lines, Figures 7B and 7C), bypassing the PEL. This phenomenon was also
272 evident in other EM images (Figures 1C and Figure 2, box 1). PBL-mediated sealing
273 is not always complete. When the PBL was not accessible or only loosely covered
274 membrane-free regions, minor cytoplasmic leakage occurred (Figure 7D). In cases
275 where PBL sealing was ineffective or absent, cytoplasmic material appeared to be
276 retained within a confined region, likely by the PEL (Figure 7D). However, the
277 mechanisms by which extracellular matrix components protect the exposed
278 cytoplasmic region remain unknown.

279

280 **Discussion**

281 In this study, we discovered that the plasma membrane of *C. elegans* embryonic cells
282 undergo rupture at metaphase. Following this rupture, the detached sister membranes
283 extend rather independently from each other to complete cytokinesis. To date, the
284 ultrastructural dynamics of plasma membrane integrity during cell division remained
285 unexplored in other species. We anticipate that our findings will catalyze comparative
286 studies across different species or under various pathological conditions, to determine
287 whether this mechanism represents a fundamental paradigm or a context-specific

288 strategy. Our work established the first mechanistic framework to guide such future
289 investigations.

290 **The advantage of membrane rupture and independent sister membrane**
291 **extension**

292 Cell division involves both nuclear and cytoplasmic division. However, due to the
293 difficulty of visualizing cell boundaries in living embryos, previous studies in *C.*
294 *elegans* have largely emphasized nuclear events. Here, we observed that early *C.*
295 *elegans* embryonic cells can contain three or four nuclei within a shared cytoplasm,
296 indicating that cytoplasmic division may be uncoupled from nuclear division. This
297 phenomenon is not unique to *C. elegans*—it has also been reported in other species
298 such as *Drosophila*, where the early embryo undergoes 13 rapid nuclear divisions
299 without cytokinesis before cellularization occurs. It has been proposed that by
300 minimizing or delaying cytokinesis, embryos can accelerate nuclear multiplication,
301 thereby supporting the rapid pace of early development. In this context, the embryonic
302 cells of *C. elegans* appear to adopt a notably rapid—though seemingly risky—strategy
303 for cell proliferation, yet one with clear developmental benefits.

304 First, membrane rupture may help alleviate the rise in intracellular pressure
305 during division (Stewart et al., 2011; Hiramoto, 1963). We observed that the size of
306 membrane discontinuities appeared to peak during metaphase, primarily around the
307 equatorial plane-consistent with localized pressure surges at this stage. Notably,
308 ruptures were also detected in tri-nucleated cell clusters, where all three cells
309 exhibited membrane discontinuities during late cytokinesis. This suggests that even

310 though the relative size of the ruptures decreases as mitosis proceeds, membrane
311 discontinuities may persist throughout the cell cycle. Maintaining an opening in the
312 plasma membrane during division likely reduces internal pressure, thereby conserving
313 energy and resources that would otherwise be expended on resisting membrane
314 tension. These conserved resources could then be redirected toward essential
315 processes such as chromosome segregation and membrane synthesis—a particular
316 advantage for rapidly dividing embryonic cells.

317 Of note, 3D reconstruction revealed that the metaphase rupture does not fully
318 bisect the membrane (Figure 2). However, given the limitations of our EM
319 sampling—neither random nor continuous imaging provides complete coverage—we
320 cannot exclude the possibility that some ruptures completely sever the membrane.
321 Regardless of the extent of separation, the rupture produces two distinct membrane
322 domains. Since this occurs as early as metaphase, before nuclear or cytoplasmic
323 division, the physical independence of the plasma membranes may serve as an early
324 marker of nascent daughter cells, preceding other cellular landmarks.

325 Following membrane rupture, the prospective sister membranes become
326 separated, raising the question of how cytokinesis proceeds with severed membranes.
327 Analysis of single EM sections revealed classical membrane invagination in only a
328 few cases (6 out of 51; Figure 3A). Notably, one such instance occurred during the
329 transition from a one-cell to a two-cell embryo. This suggests that while a subset of *C.*
330 *elegans* embryonic cells employs the membrane invagination and extension model,
331 the majority do not. Interestingly, membrane discontinuities were observed in one-cell
332 embryos (Figure S1), indicating that membrane rupture can co-occur with
333 invagination. Alternatively, in dividing cells, the back-to-back invagination may be

334 transient and may subsequently transition to free-ended extension. At present,
335 distinguishing between these hypotheses remains challenging. A definitive resolution
336 will likely require advanced imaging techniques capable of high-resolution, real-time
337 visualization at the EM level.

338 Unlike a continuous bilayer, a free-ended membrane offers greater flexibility
339 during cytokinesis. Without being physically constrained by its sister, each membrane
340 can extend in different directions as needed. This independence may be particularly
341 advantageous in accommodating asynchrony between nuclear and cytoplasmic
342 division, as seen in early *C. elegans* embryos where multinucleated cells form through
343 incomplete cytokinesis. In such cases, independent membrane growth from two
344 directions facilitates cytoplasmic separation more effectively than a single continuous
345 membrane would allow. Such autonomous movement may also explain the divergent
346 orientations of sister membranes frequently observed in EM sections.

347 The expansion of the plasma membrane is generally driven by vesicle fusion. In
348 this study, vesicles seem observed randomly distributed beneath the extending sister
349 membranes. EM analysis further showed no morphological differences between
350 vesicles near cytosol-immersed regions and those at conventional membrane sites.
351 Since vesicles can fuse with the membrane at various locations, we speculate that
352 membrane growth may be enhanced under these conditions—potentially accelerating
353 cell cleavage during early embryogenesis. However, this remains speculative and
354 requires further experimental validation.

355 Finally, when the separated membrane edges meet within daughter cells, full
356 cytoplasmic separation is achieved. In the classical invagination-extension model,
357 cytokinesis requires both membrane scission and fusion. In the detached-membrane

358 mode described here, however, cytokinesis proceeds without a continuous membrane
359 structure. This raises important questions: Is membrane scission dispensable in this
360 context? Could bypassing scission accelerate cell separation? If so, might such a
361 mechanism offer a selective advantage during rapid embryonic development? These
362 questions remain open and merit further investigation.

363 **Limitations and perspectives**

364 In this study, the application of HPF-TEM has enabled unprecedented ultrastructural
365 visualization of dividing cell surfaces. Our findings reveal a cytoplasmic division
366 mechanism that challenges current models and raises important new questions
367 regarding the plasticity of cytokinesis.
368 HPF-TEM offers a significant advantage for membrane studies by capturing
369 cellular structures in a near-native state. Through ultra-rapid freezing under high
370 pressure, it suppresses ice crystal formation and preserves water in a vitreous state,
371 thereby minimizing chemical artifacts and maintaining the integrity of lipids and
372 proteins. This method provides a faithful snapshot of membrane architecture and
373 dynamics(Moor et al., 1980). In our experiments, the consistent observation of limited
374 number of membrane discontinuities-generally one per dividing cell-that are closely
375 associated with cell division strongly suggests these are genuine biological structures
376 rather than preparation-induced artifacts. While one might argue that such features
377 could reflect EM-related artifacts specific to the plasma membrane during division,
378 the correlative evidence presented here supports their biological relevance.

379 Using fluorescence-labeled membrane markers, we identified membrane ruptures
380 and free-ended sister membrane structures in live embryos (Figure 6). Similar
381 “abnormal” or “fuzzy” membrane signals have in fact been reported

382 previously(Harrell and Goldstein, 2011). However, interpretating these structures has
383 remained challenging for both technical and conceptual reasons. Technically, the
384 rapid kinetics of membrane extension-about 10-30 seconds during metaphase and less
385 than 3 minutes during cytokinesis-combined with cell motility, introduce inherent
386 spatiotemporal ambiguities. Conceptually, the longstanding dominance of the
387 membrane invagination model has likely shaped—and potentially constrained—
388 interpretations of membrane dynamics. This paradigm may have led researchers to
389 prioritize observations consistent with invagination, while dismissing ambiguous
390 structures such as free-ended extensions as artifacts, rather than considering them as
391 potential elements of alternative mechanisms. Furthermore, theoretical and
392 computational models of cytokinesis have largely been built on invagination-centric
393 assumptions, further narrowing the conceptual framework.

394 A key limitation is our current inability to capture 3D dynamics of these
395 membrane structures in real time, a challenge that awaits imaging technologies with
396 sufficient spatiotemporal resolution at near -EM levels.

397 Therefore, while our findings propose a transformative model for cytokinesis,
398 they open a new field of inquiry. Fully validating this mechanism and exploring its
399 conservation and implications will require an integrated approach combining
400 advanced live-cell imaging, biophysical modeling, and genetic tools.

401 **Methods and Materials**

402 **Examination of *C. elegans* embryonic cells**

403 Wild-type N2 worms were cultured on OP50-seeded NGM plates at 22°C (Brenner,
404 1974). To obtain images of early embryos, gravid hermaphrodites were collected and
405 sectioned. At low magnification (×4000), individual embryonic cells were identified
406 by the presence of a nucleus. In sections where the nucleus was not visible,
407 cytoplasmic regions—whether covered or not covered by plasma membrane—were
408 counted as individual cells if they were separated from surrounding cells. A total of
409 425 cells were examined (summarized in Figure 1C), with one EM section analyzed
410 per cell. For embryos with fewer than 10 cells (one or two rows of cells), every cell in
411 the given section was examined. For embryos with three or more rows of cells, only
412 cells at the periphery were analyzed. At higher magnification (×30,000), the entire
413 surface of each cell was examined, revealing 159 cells with one or more membrane
414 openings. Higher magnification improved the resolution of cytoplasmic continuity,
415 reducing potential misidentification of multinucleated cells or interconnected
416 cytoplasmic regions that might have been miscounted at lower magnification. A total
417 of 60 early embryos were serially sectioned as completely as possible, with each
418 embryo yielding at least 20 sections. While Figure 1C presents summary data, images
419 from additional sections were also used for further analyses. Since these additional
420 sections may capture different cells, the total number of embryonic cells examined
421 likely exceeds 425.

422 Additionally, we examined eight embryos laid outside the worm. Among these,
423 four pre-comma stage embryos each contained at least one MO-positive cell. In
424 another pre-comma stage embryo, no MOs were detected after examining 17 cells.

425 Analysis of one comma-stage embryo (19 cells examined) and two 1.5-fold-stage
426 embryos (>30 cells analyzed each) revealed no MOs.

427 **Identification of MOs**

428 The entire cell surface of individual embryonic cells was examined using electron
429 microscopy at 30,000× magnification. The isolated cytoplasmic regions without
430 plasma membrane coverage were defined as MOs. Sites where the plasma membrane
431 terminated and reappeared were marked as putative MOs. In periphery region of
432 worm embryos, in the non-plasma-membrane-covering regions, the PEL was
433 generally absent, while the PBL typically extended over the exposed cytoplasmic
434 surface. Plasma membranes often appeared wrinkled, whereas cytoplasmic regions
435 covered by the PBL exhibited a smoother appearance. Smooth, non-plasma-
436 membrane-covered regions overlaid by the PBL are readily identifiable as MOs.
437 When exposed cytoplasm was not tightly covered by the PBL, cytoplasmic leakage—
438 still confined to a specific area by the PEL—could also indicate a MO. Given the
439 variable morphology and frequent cytoplasmic leakage, membrane discontinuity size
440 could not serve as a reliable criterion for defining MOs. However, to ensure
441 robustness in our analysis, we considered only linear membrane discontinuities
442 exceeding 200 nm as genuine openings. Each MO was examined independently at
443 least three times. When necessary, adjacent sections were also reviewed to conform an
444 MO's presence, and identification was finalized only after all three assessments were
445 positive.

446 **High-pressure freezing and transmission electron microscopy**

447 Basic protocols for high-pressure freezing of a range of organisms, including *C.*
448 *elegans*, have been described (Weimer, 2006; McDonald, 2007; Manning and
449 Richmond, 2015). Briefly, adult worms were loaded into carriers and cryofixed using

450 a Leica Microsystems EM ICE high-pressure freezer, followed by automatic cooling
451 in liquid nitrogen. The carriers used for freezing (Leica Microsystems, Germany;
452 catalog nos. 16770153 and 16770152) were coated with a non-stick layer of 1-
453 hexadecene (Sigma-Aldrich). After high-pressure freezing (HPF), the samples were
454 transferred under liquid nitrogen to a Leica AFS-2 freeze-substitution unit and
455 incubated at −90°C for 72 h in a freeze-substitution solution consisting of acetone
456 with 2% (wt/vol) osmium tetroxide. The temperature was then raised at a rate of
457 8°C/h for 4 h, held at −60°C for 12 h, increased again at 5°C/h for 6 h, held at −30°C
458 for 10 h, and finally raised to 10°C at a rate of 4°C/h for 10 h. Samples were washed
459 four times in acetone, stained with 1% uranyl acetate for 1 h, and rinsed three times
460 with pure acetone. They were then infiltrated stepwise in increasing concentrations of
461 SPI-Chem™ resin (2:1 resin:acetone for 3 h, 1:1 for 5 h), followed by two incubations
462 in 100% fresh resin (4 h each). The samples were placed in fresh resin in embedding
463 molds and polymerized in a 60°C oven for 3 days. Ultrathin sections (60 nm) were cut
464 using a diamond knife (Diatome) on an ultramicrotome (Leica Ultracut UC7) and
465 collected on slot copper grids (EMS). The sections were visualized using a Hitachi
466 HT7700 transmission electron microscope operating at 80 kV. Images were recorded
467 with a Gatan 832 (4k × 2.7k) CCD camera. Data from four independent preparations
468 were analyzed in this study.

469 **3D reconstruction**

470 The metaphase 3D model was prepared using the following steps. First, resin blocks
471 containing gravid adults were prepared via high-pressure freezing and freeze
472 substitution. Continuous ultrathin sections (60 nm thick) were manually collected
473 using a Leica UC-7 ultramicrotome and mounted on slot grids for TEM imaging. A
474 total of 112 serial sections were collected, though 3 sections were lost due to

475 obstruction, resulting in 822 TEM images. Among these, 105 sections contained
476 metaphase-stage cell information. To examine the plasma membrane integrity, high-
477 magnification imaging was performed. Since a single high-magnification image could
478 not cover the entire cell, multiple overlapping images were captured per section and
479 stitched together using ImageJ to generate a complete composite image of the cellular
480 morphology at each section. In total, 292 images were stitched. The 105 stitched
481 images were then aligned using ImageJ, and 99 of these aligned images were used for
482 3D reconstruction using Imaris software. About a quarter of the cell lacked membrane
483 discontinuities. For this portion, we estimated its size and shape based on EM sections
484 to ensure proportional representation. Of note, single MOs smaller than 200 nm that
485 appeared continuously across more than 3 consecutive sections were considered the
486 endpoint of the membrane rupture. Based on this, the actual length of the membrane
487 rupture could be underestimated at one end, while the other end was clearly defined.
488 The ultrastructural 3D study of the tri-nucleated cell was performed using an
489 AutoCUTS device (Li et al., 2017) and a Helios Nanolab 600i dual-beam scanning
490 electron microscope (FEI). Adult worms were treated with high-pressure freezing,
491 freeze-substitution, and embedding as described above. Subsequently, 351 serial
492 sections (60 nm thick) were collected using the AutoCUTS device, and scanning
493 electron microscopy imaging was performed. All datasets were analyzed using
494 IMARIS 8 software. After Z-stacks were aligned, the membrane rupture was manually
495 traced and reconstructed.

496 **Live imaging of plasma membrane dynamics using GFP::PH**

497 The plasma membrane was labeled using GFP::PH(PLC1δ1). The strain carrying this
498 marker was obtained from the Caenorhabditis Genetics Center and was originally
499 generated in Dr. Karen Faye Oegema's laboratory. Gravid adult hermaphrodites

500 expressing this marker were collected and washed with M9 buffer. Embryos were then
501 released from the gravid adult worms using a 1 mL syringe needle and transferred
502 onto a 2% agarose pad. Fluorescence imaging was performed on a Zeiss LSM-980
503 microscope with a 63×/1.42 oil objective. Only one embryo at a time was imaged,
504 starting at the 2- to 4-cell stage. Images were acquired at 4 or 8-second intervals, with
505 total imaging duration typically kept under 30 minutes to ensure embryo viability.

Acknowledgements

We thank the Center for Biological Imaging at the Institute of Biophysics, Chinese Academy of Sciences (CAS) for technical support. We are grateful to Drs. John White, Andrew Chisholm, and Zhuo Du for their encouragement and insightful suggestions. This work was supported by grants from the National Key R&D Program of China (2024YFA1803401, 2021YFA0805802, and 2024YFA1306100) and the Natural Science Foundation of China (32170790 and 32321004).

Author contributions

Study concept and design: MD, JL. EM analyses: JL, TH, MD. Drafting and major editing of original manuscript: MD, JL, TH, XH. All authors reviewed, revised, and approved the final version of the paper.

Competing interests

The authors declare no competing interests.

Correspondence and requests for materials should be addressed to Mei Ding

523 **Figure legends**

524 **Figure 1. Membrane discontinuities in *C. elegans* embryonic cells.**

525 A, Schematic drawing of a metaphase cell and the classical membrane invagination
526 model. B, Schematic drawing of a metaphase cell with a ruptured plasma membrane
527 and a cytokinesis model showing that the detached sister membranes mediate
528 membrane extension in *C. elegans* embryonic cells. C, A membrane opening (MO,
529 indicated by white dashed line) in an embryonic cell at the embryo's periphery. D,
530 Membrane openings in the embryo's central regions. Yellow arrows point to single
531 plasma membranes (SPM) traversing the cytoplasm. Plasma membranes are in blue.
532 E, Summary of the single EM section survey of plasma membrane continuity. Orange
533 lines outline the plasma membranes. Solid gray circles/ellipses enclosed by dashed
534 lines represent evenly stained nucleoid regions. Condensed chromosome structures
535 are colored gray-blue. Light brown areas represent cytoplasmic regions.

536

537 **Figure 2. Metaphase membrane rupture.**

538 A, Membrane discontinuities or openings (MO) (white dashed line) in a metaphase
539 cell (MC). Enlarged views of the boxed regions (1, 2 and 3) are shown. Yellow arrows
540 indicate the plasma membrane (PM). B, MOs (marked by 1 and 2) are detected in
541 anaphase (AC) and other early embryonic cells; enlarged views of the MOs are shown
542 (white dashed lines). All yellow arrows point from the interior of the cell toward the
543 plasma membrane. C and D, Three-dimensional (3D) reconstruction of a metaphase
544 cell. Representative EM images are shown in (C). Purple lines outline the plasma
545 membranes. White dashed lines outline the exposed cytoplasmic region. Blue lines
546 outline the condensed chromosome region. D, The 3D reconstruction of the
547 metaphase cell. The plasma membrane (PM) and condensed chromosome region are

548 displayed.

549

550 **Figure 3. The detached severed sister membranes.**

551 A, Representative image of a classical back-to-back membrane arrangement. B,
552 Representative image of detached severed sister membranes. Diagrams of the
553 corresponding cytokinesis models are displayed on the right. C, Tips of two detached
554 sister membranes. D, Cytosol-immersed single membranes separating the cytoplasmic
555 regions of two adjacent cells. Enlarged views of regions 1 and 2 are shown below.
556 Plasma membranes (PM) are indicated by yellow arrows (A, B and D) or blue lines.
557 Asterisks indicate membrane tips.

558

559 **Figure 4. Cellular vesicles on detached sister membranes.**

560 A, A vesicle localized at the tip of a cytosol-immersed membrane. B, Vesicles
561 clustering near the cytosol-immersed region of sister membranes. Contact or fusion
562 between vesicles and membranes is indicated. The rectangular inset shows an
563 enlarged view of a gap junction (GJ) plaque. C, Putative fusion events between
564 vesicles and free-ended membranes. D, Vesicles found near the separated sister
565 membranes. Plasma membranes are in blue.

566

567 **Figure 5. Membrane rupture on a tri-nucleated cell.**

568 A, The 3D model of a tri-nucleated cell showing the membrane rupture (black). B,
569 Reconstruction of the membrane ruptures and adjacent plasma membranes. Individual

570 membranes, each associated with a distinct nucleus, are color-coded (blue, yellow,
571 and purple). C and D, Membrane openings (MO, dashed white lines) arise either from
572 separation between sister membranes (C) or between the severed membrane edges of
573 the same cell (D). E, In a single EM section, the multiple openings originate from the
574 same rupture. F and G, The opposing severed edges are close to each other in the
575 yellow, purple and blue cells. Plasma membranes (PM) are indicated in blue.
576 Asterisks indicate membrane tips. H, Schematic diagram of the formation of cells
577 with three or four nuclei.

578 **Figure 6. Detection of membrane disruptions by optical microscopy.**
579 A, The putative membrane rupture and extension (*). B, Two extending free-ended
580 sister membranes (*). Insets are enlarged views. C, Possible free-ended edges of
581 detached membranes, probably from multiple cells (*). Below are proposed models
582 illustrating the membrane disruptions that could explain the anomalous GFP signals.
583 Images were taken at 4-second intervals for (A and B) and 8-second intervals for (C).
584 Green signal is GFP::PH(PLC1δ1).
585

586 **Figure 7. The exposed cytoplasmic regions are covered by extracellular matrix**
587 **layers.**
588 A-C, The exposed cytoplasmic region is covered by the permeability barrier layer
589 (PBL, red triangles and red dashed lines). PM, plasma membrane (yellow arrows and
590 blue lines). The boxed region in (A) is enlarged in (B), and the boxed region in (B) is
591 enlarged in (C). D, The exposed cytoplasmic region can also be confined by the peri-
592 embryonic layer (PEL).

593 **Supplementary Figure Legends**

594 **Figure S1. Membrane discontinuities in externally laid *C. elegans* embryos.**

595 A, An externally laid embryos with a membrane discontinuity (white box). B, Higher-
596 magnification view of the membrane opening (MO) (white dashed line). Yellow
597 arrow, plasma membrane; asterisk (*), condensed chromosome.

598

599 **Figure S2. The wide distribution of cells with membrane discontinuities in early**
600 ***C. elegans* embryos.**

601 A, Schematic diagram of *C. elegans* embryogenesis. B-N, Representative low-
602 magnification EM images of early embryos within adult hermaphrodites. Red lines
603 outline cells contain membrane openings. In (F), a tri-nucleated cell is marked with &.
604 (L) and (M) show embryos during the transition from the one-cell to the two-cell
605 stage.

606

607 **Figure S3. Membrane discontinuities in cells during mitosis.**

608 A-C, Membrane discontinuities or openings (MO, white or black dashed lines) in cells
609 at metaphase (A), anaphase (B) or telophase (C). Yellow arrows points to plasma
610 membranes (PMs).

611

612 **Video S1. 3D reconstruction of the metaphase cell in Figure 2.**

613 The plasma membrane is shown in red, the condensed chromosome is in blue, and
614 exposed cytoplasm is in green.

615

616 **Video S2. 3D reconstruction of the tri-nucleated cell in Figure 5.**

617 3D reconstruction of membrane ruptures and adjacent plasma membranes. Individual

membranes, each associated with a distinct nucleus, are color-coded (purple, yellow, or blue).

Bao, Z., Z. Zhao, T.J. Boyle, J.I. Murray, and R.H. Waterston. 2008. Control of cell cycle timing during C. elegans embryogenesis. *Developmental Biology*. 318:65–72. doi:10.1016/j.ydbio.2008.02.054.

Bembenek, J.N., C.T. Richie, J.M. Squirrell, J.M. Campbell, K.W. Eliceiri, D. Poteryaev, A. Spang, A. Golden, and J.G. White. 2007. Cortical granule exocytosis in *C. elegans* is regulated by cell cycle components including separase. *Development*. 134:3837–3848. doi:10.1242/dev.011361.

Benenati, G., S. Penkov, T. Müller-Reichert, E.V. Entchev, and T.V. Kurzchalia. 2009. Two cytochrome P450s in Caenorhabditis elegans are essential for the organization of eggshell, correct execution of meiosis and the polarization of embryo. *Mechanisms of Development*. 126:382–393. doi:10.1016/j.mod.2009.02.001.

Brenner, S. 1974. THE GENETICS OF *CAENORHABDITIS ELEGANS*. *Genetics*. 77:71–94. doi:10.1093/genetics/77.1.71.

Deppe, U., E. Schierenberg, T. Cole, C. Krieg, D. Schmitt, B. Yoder, and G. Von Ehrenstein. 1978. Cell lineages of the embryo of the nematode Caenorhabditis elegans. *Proc. Natl. Acad. Sci. U.S.A.* 75:376–380. doi:10.1073/pnas.75.1.376.

Edgar, L.G., and J.D. McGhee. 1988. DNA synthesis and the control of embryonic gene expression in C. elegans. *Cell*. 53:589–599. doi:10.1016/0092-8674(88)90575-2.

Gerien, K.S., and J.-Q. Wu. 2018. Molecular mechanisms of contractile-ring constriction and membrane trafficking in cytokinesis. *Biophys Rev*. 10:1649–1666. doi:10.1007/s12551-018-0479-3.

Harrell, J.R., and B. Goldstein. 2011. Internalization of multiple cells during C. elegans gastrulation depends on common cytoskeletal mechanisms but different cell polarity and cell fate regulators. *Developmental Biology*. 350:1–12. doi:10.1016/j.ydbio.2010.09.012.

Hiramoto, Y. 1963. Mechanical properties of sea urchin eggs. I. Surface force and elastic modulus of the cell membrane. *Experimental Cell Research*. 32:59–75. doi:10.1016/0014-4827(63)90069-7.

Li, X., G. Ji, X. Chen, W. Ding, L. Sun, W. Xu, H. Han, and F. Sun. 2017. Large scale three-dimensional reconstruction of an entire Caenorhabditis elegans larva using AutoCUTS-SEM. *Journal of Structural Biology*. 200:87–96. doi:10.1016/j.jsb.2017.09.010.

Manning, L., and J. Richmond. 2015. High-Pressure Freeze and Freeze Substitution

656 Electron Microscopy in C. elegans. *In* C. elegans. D. Biron and G. Haspel,
657 editors. Humana Press, Totowa, NJ. 121–140.

658 McDonald, K. 2007. Cryopreparation Methods for Electron Microscopy of Selected
659 Model Systems. *In* Methods in Cell Biology. Elsevier. 23–56.

660 Modern Electron Microscopy Methods for C. elegans. 2012. *In* Methods in Cell Biology.
661 Elsevier. 93–149.

662 Moor, H., G. Bellin, C. Sandri, and K. Akert. 1980. The influence of high pressure
663 freezing on mammalian nerve tissue. *Cell Tissue Res.* 209.
664 doi:10.1007/BF00237626.

665 Olson, S.K., G. Greenan, A. Desai, T. Müller-Reichert, and K. Oegema. 2012.
666 Hierarchical assembly of the eggshell and permeability barrier in *C. elegans*.
667 *Journal of Cell Biology*. 198:731–748. doi:10.1083/jcb.201206008.

668 Pintard, L., and B. Bowerman. 2019. Mitotic Cell Division in *Caenorhabditis elegans*.
669 *Genetics*. 211:35–73. doi:10.1534/genetics.118.301367.

670 Pollard, T.D., and B. O'Shaughnessy. 2019. Molecular Mechanism of Cytokinesis.
671 *Annu. Rev. Biochem.* 88:661–689. doi:10.1146/annurev-biochem-062917-
672 012530.

673 Rappleye, C.A., A.R. Paredez, C.W. Smith, K.L. McDonald, and R.V. Aroian. 1999.
674 The coronin-like protein POD-1 is required for anterior-posterior axis formation
675 and cellular architecture in the nematode Caenorhabditis elegans. *Genes &*
676 *Development*. 13:2838–2851. doi:10.1101/gad.13.21.2838.

677 Schierenberg, E., and B. Junkersdorf. 1992. The role of eggshell and underlying
678 vitelline membrane for normal pattern formation in the early C. elegans embryo.
679 *Roux's Arch Dev Biol*. 202:10–16. doi:10.1007/BF00364592.

680 Stein, K.K. 2018a. The C. elegans eggshell. *WormBook*. 1–36.
681 doi:10.1895/wormbook.1.179.1.

682 Stewart, M.P., J. Helenius, Y. Toyoda, S.P. Ramanathan, D.J. Muller, and A.A. Hyman.
683 2011. Hydrostatic pressure and the actomyosin cortex drive mitotic cell
684 rounding. *Nature*. 469:226–230. doi:10.1038/nature09642.

685 Sulston, J.E., E. Schierenberg, J.G. White, and J.N. Thomson. 1983. The embryonic cell
686 lineage of the nematode Caenorhabditis elegans. *Developmental Biology*.
687 100:64–119. doi:10.1016/0012-1606(83)90201-4.

688 Weimer, R.M. 2006. Preservation of *C. elegans* Tissue Via High-Pressure Freezing and
689 Freeze-Substitution for Ultrastructural Analysis and Immunocytochemistry. *In*
690 C. elegans. Humana Press, New Jersey. 203–222.

Zhang, Y., J.M. Foster, L.S. Nelson, D. Ma, and C.K.S. Carlow. 2005. The chitin synthase genes chs-1 and chs-2 are essential for C. elegans development and responsible for chitin deposition in the eggshell and pharynx, respectively. *Developmental Biology*. 285:330–339. doi:10.1016/j.ydbio.2005.06.037.

Zhu, J., S.M. Lam, L. Yang, J. Liang, M. Ding, G. Shui, and X. Huang. 2022. Reduced phosphatidylcholine synthesis suppresses the embryonic lethality of seipin deficiency. *Life Metabolism*. 1:175–189. doi:10.1093/lifemeta/loac021.

Figure 1

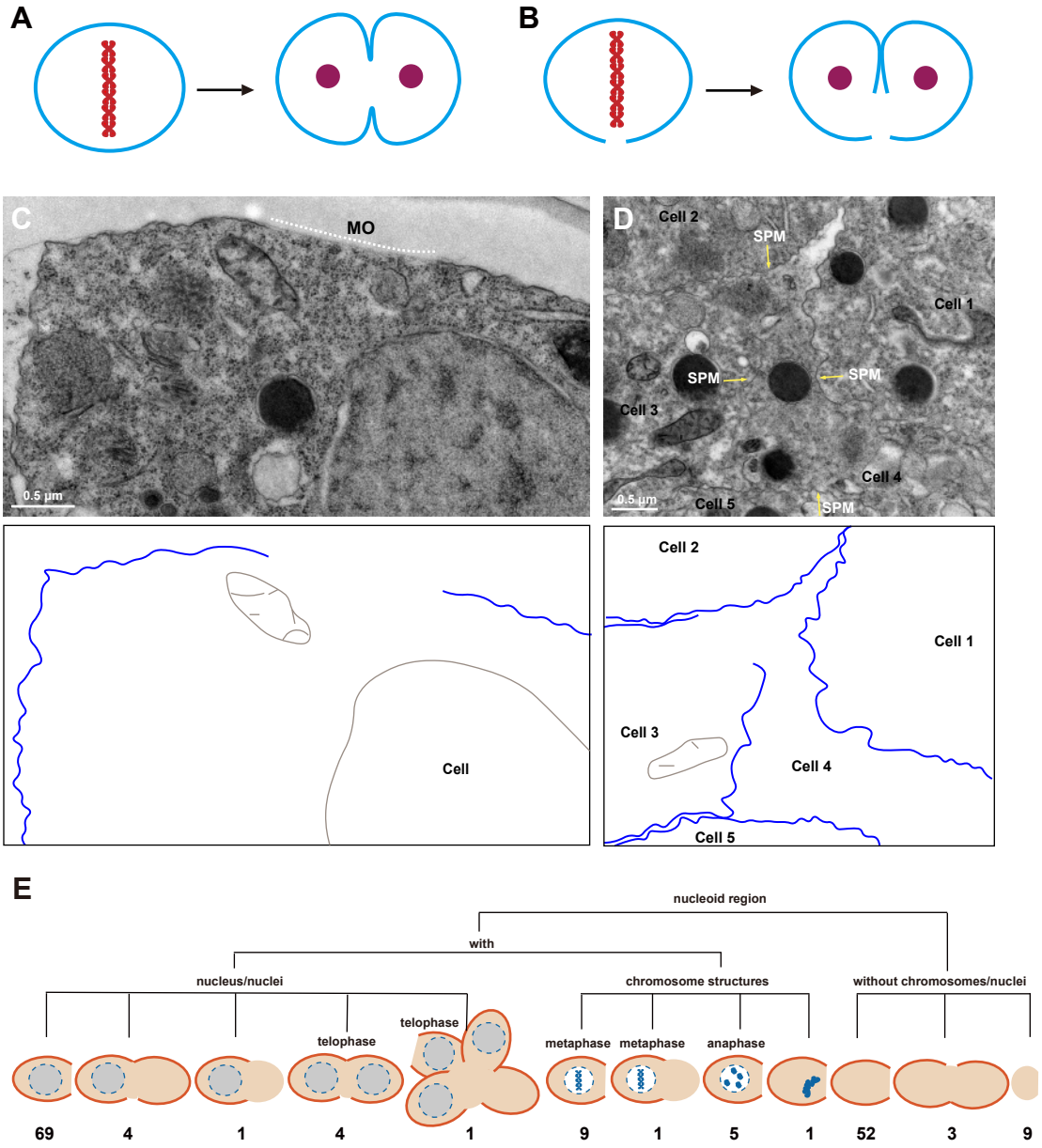
A
B
C
MO
0.5 µm
D
Cell 2
SPM
Cell 1
SPM
SPM
Cell 3
Cell 4
0.5 µm
Cell 5
SPM
Cell
Cell 2
Cell 1
Cell 3
Cell 4
Cell 5
E
nucleoid region
with
nucleus/nuclei
chromosome structures
without chromosomes/nuclei
telophase
telophase
metaphase
metaphase
anaphase
69
4
1
4
1
9
1
5
1
52
3
9

Figure 2

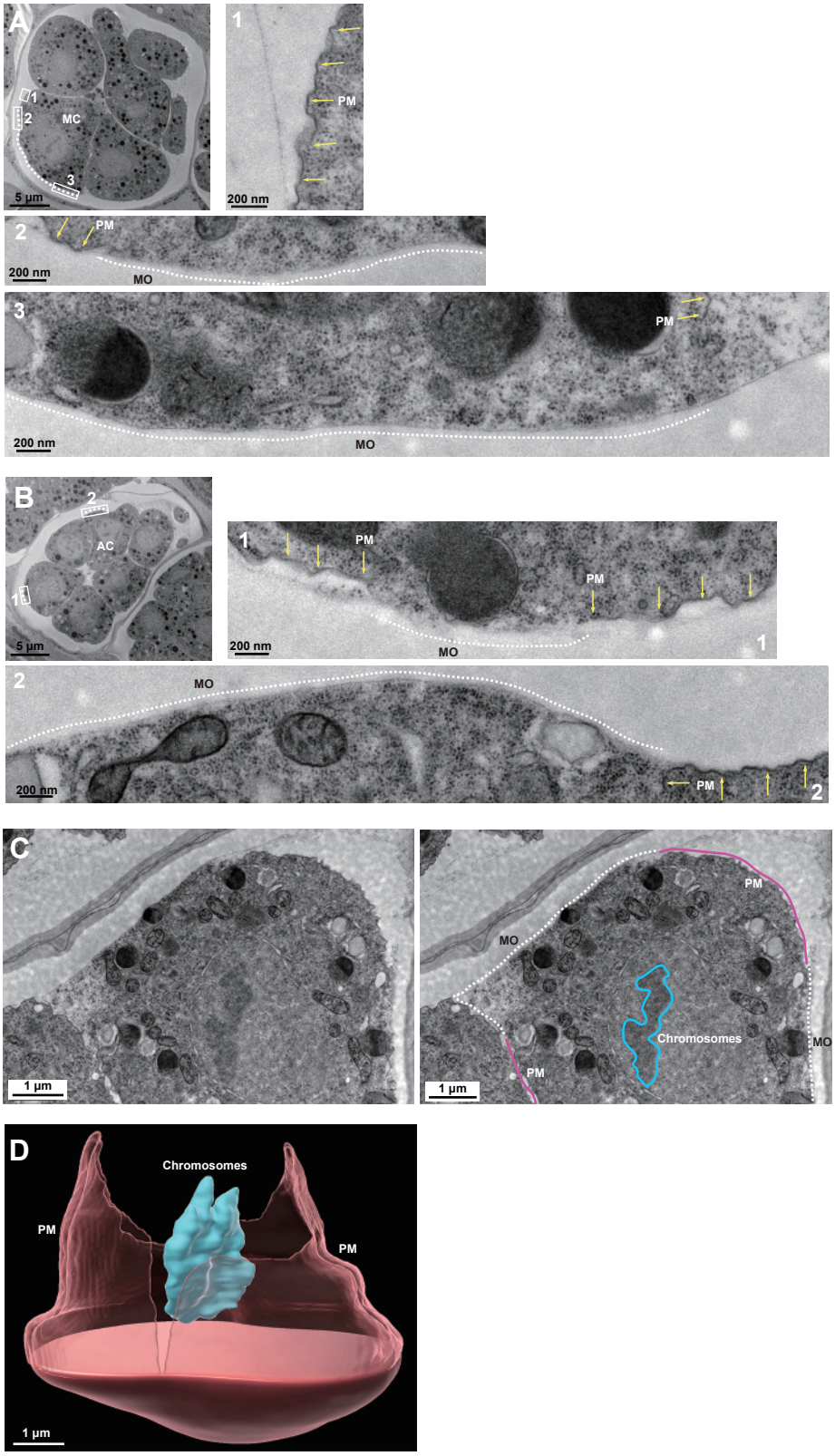
A
1
2
3
MC
5 µm
1
PM
200 nm
2
PM
200 nm
MO
3
PM
200 nm
MO
B
2
AC
1
5 µm
1
PM
PM
200 nm
MO
1
2
MO
200 nm
PM
2
C
1 µm
PM
MO
Chromosomes
MO
PM
1 µm
D
Chromosomes
PM
PM
1 µm

Figure 3

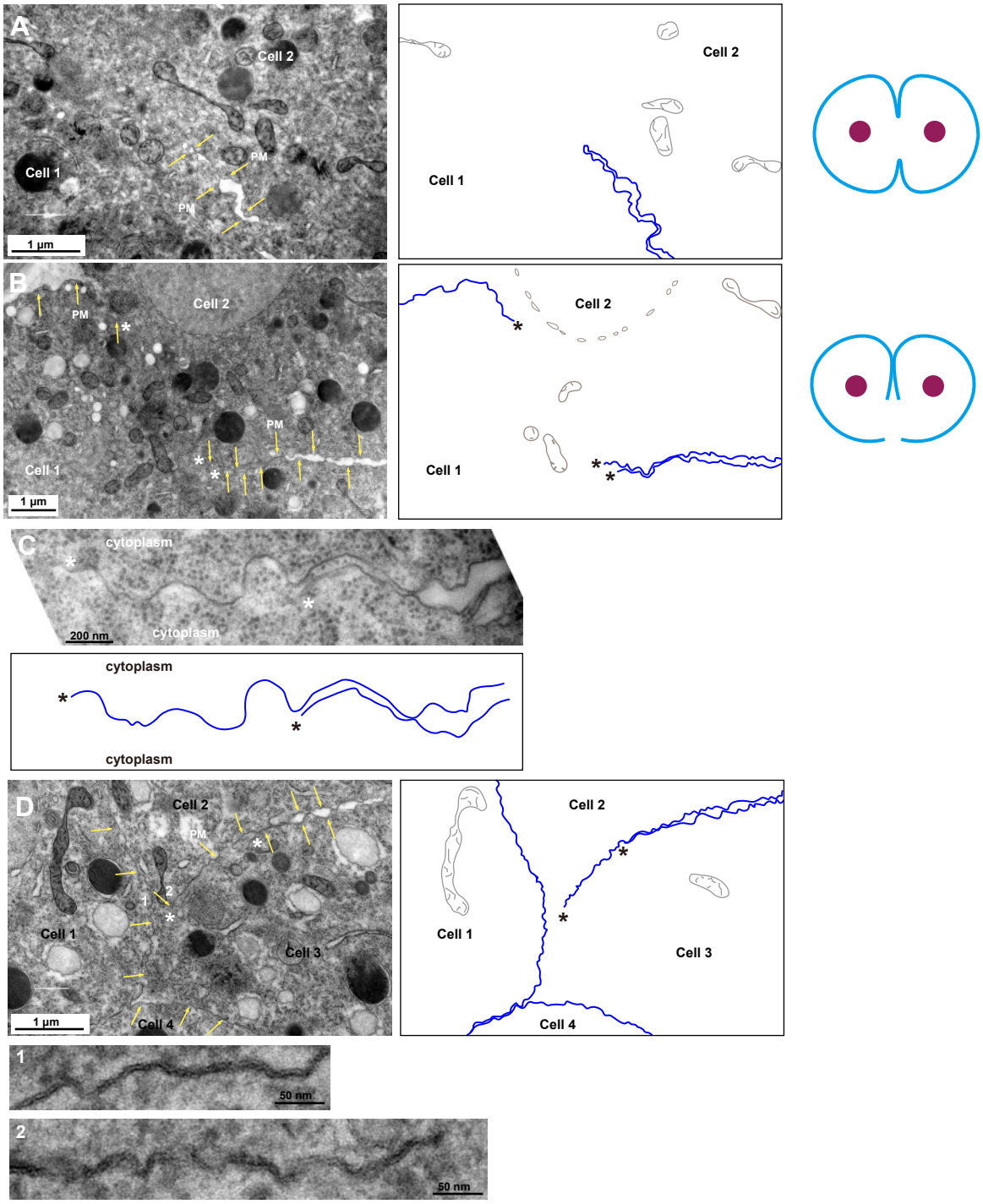
A
Cell 2
Cell 1
PM
PM
1 µm
Cell 2
Cell 1
B
PM
Cell 2
PM
Cell 1
1 µm
Cell 2
Cell 1
C
cytoplasm
200 nm
cytoplasm
cytoplasm
cytoplasm
D
Cell 2
PM
1
2
Cell 1
Cell 3
1 µm
Cell 4
Cell 2
Cell 1
Cell 3
Cell 4
1
50 nm
2
50 nm

Figure 4

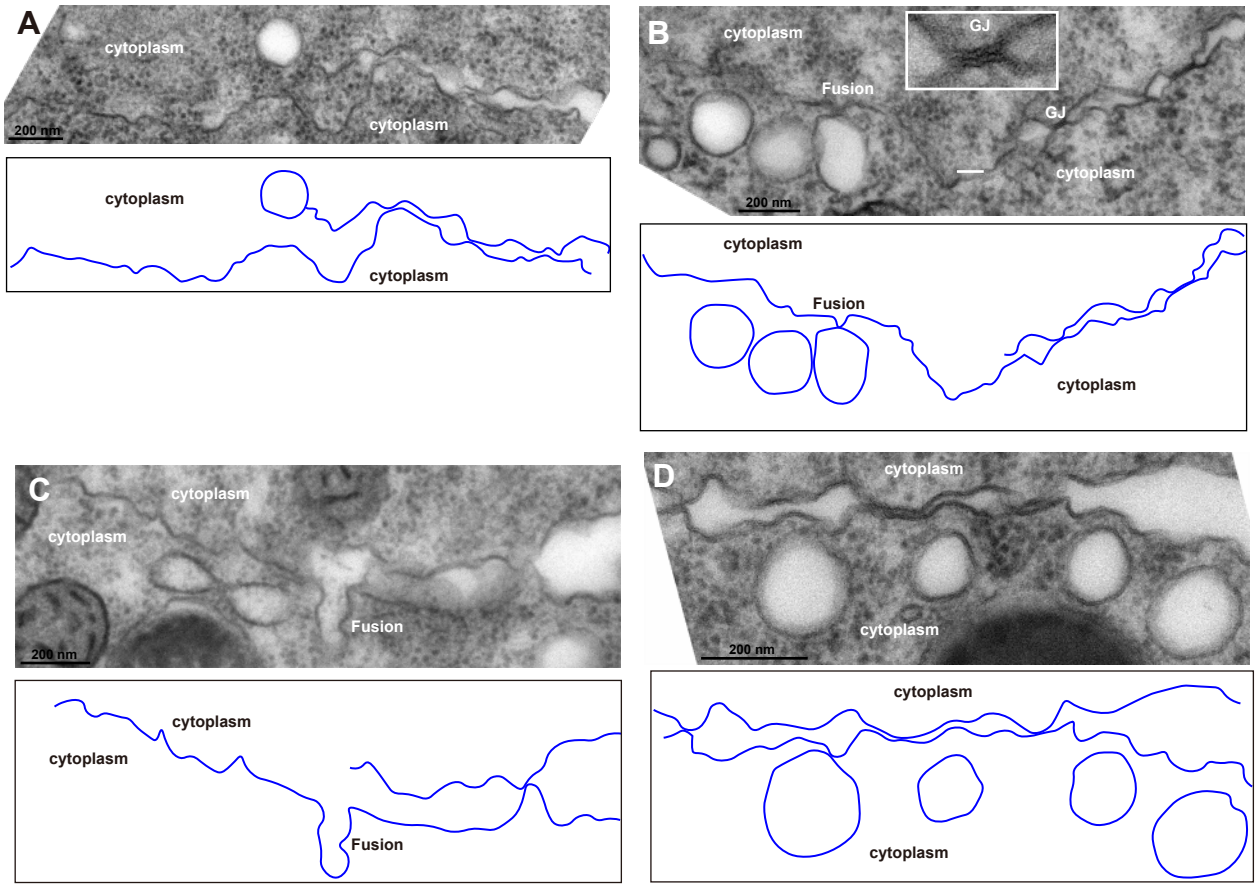
A
cytoplasm
cytoplasm
200 nm
cytoplasm
cytoplasm
B
cytoplasm
GJ
Fusion
GJ
cytoplasm
200 nm
cytoplasm
Fusion
cytoplasm
C
cytoplasm
cytoplasm
Fusion
200 nm
cytoplasm
cytoplasm
Fusion
D
cytoplasm
cytoplasm
200 nm
cytoplasm
cytoplasm

Figure 5

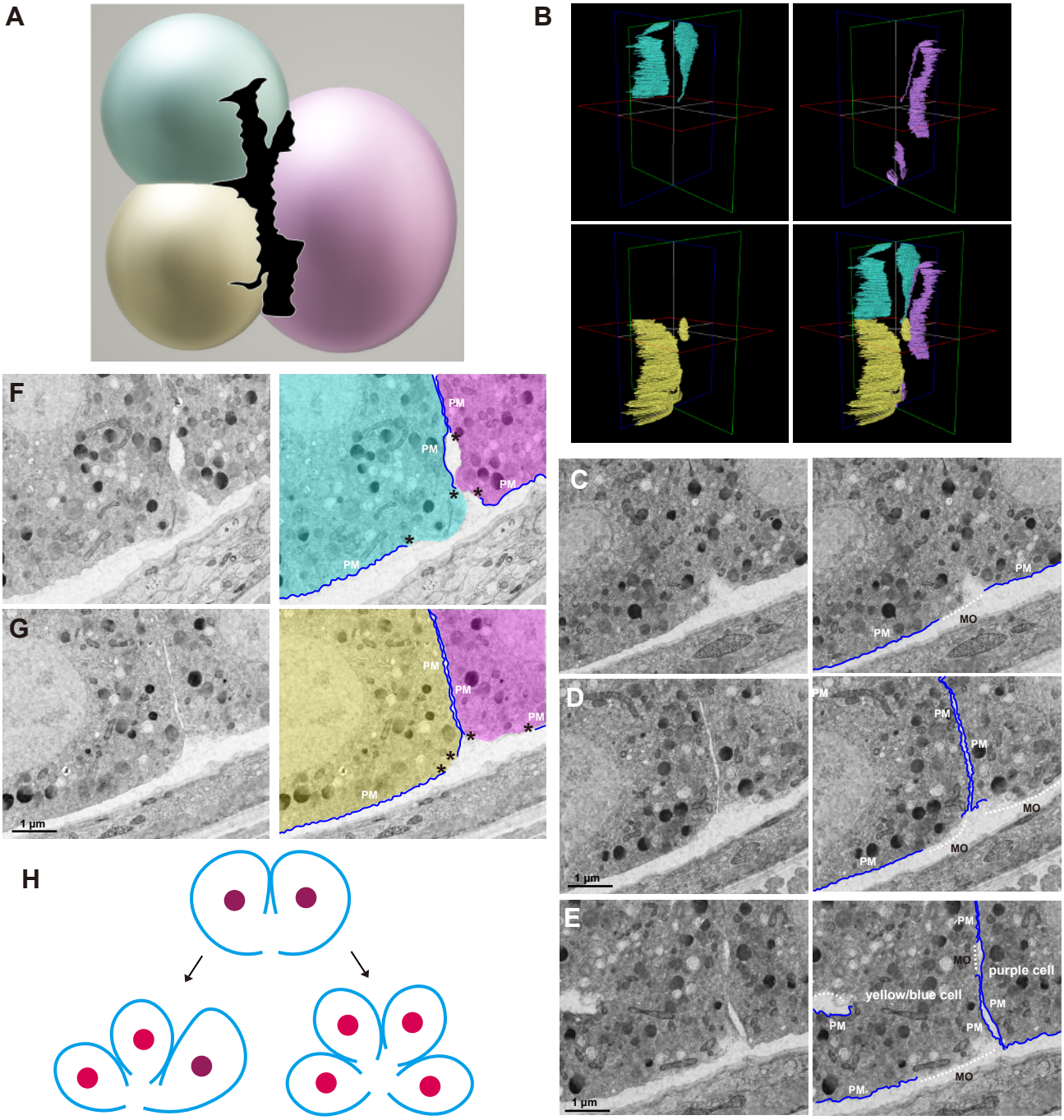

Figure 6

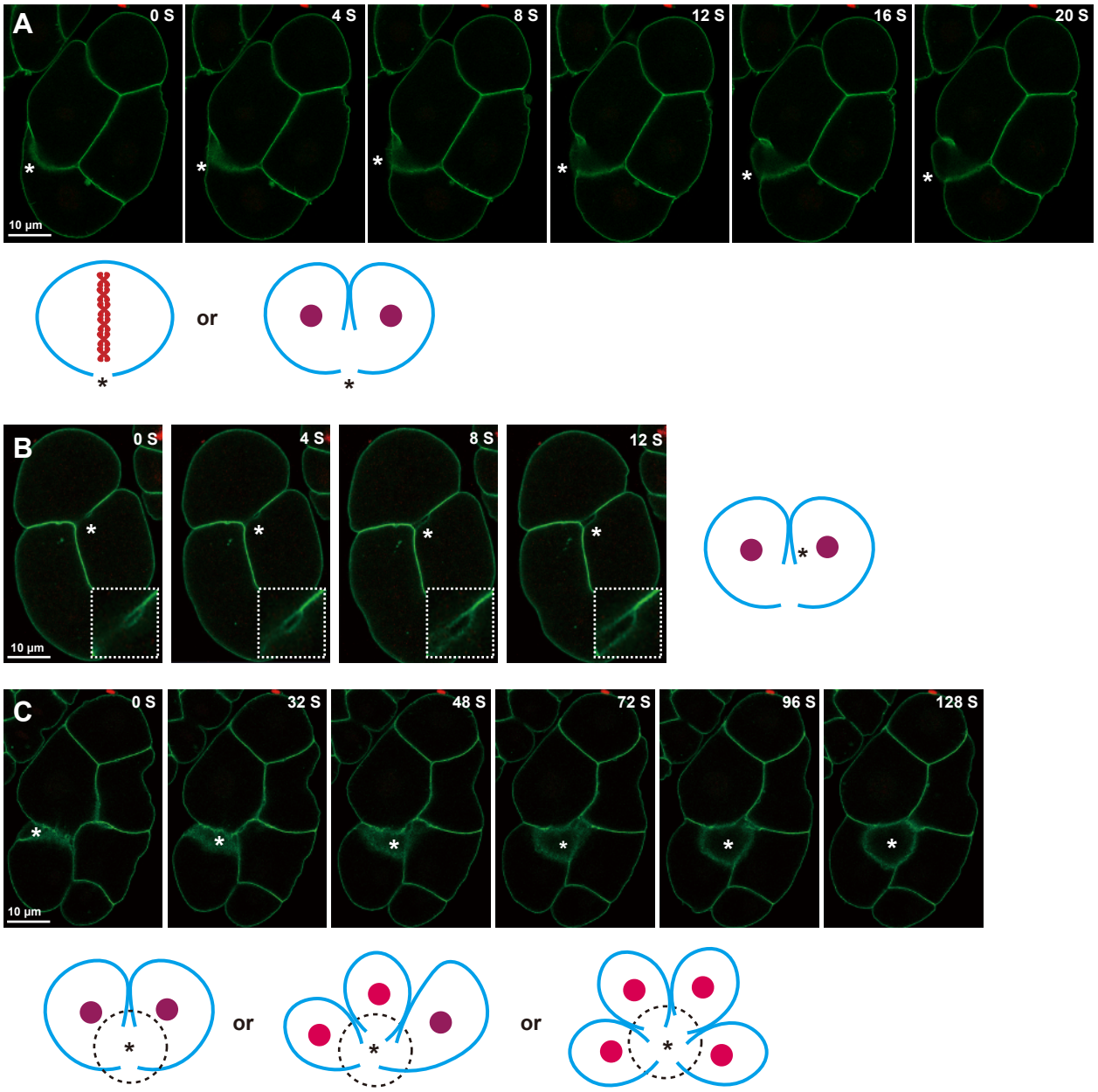
A
0 S
4 S
8 S
12 S
16 S
20 S
10 µm
or
B
0 S
4 S
8 S
12 S
10 µm
C
0 S
32 S
48 S
72 S
96 S
128 S
10 µm
or
or

Figure 7

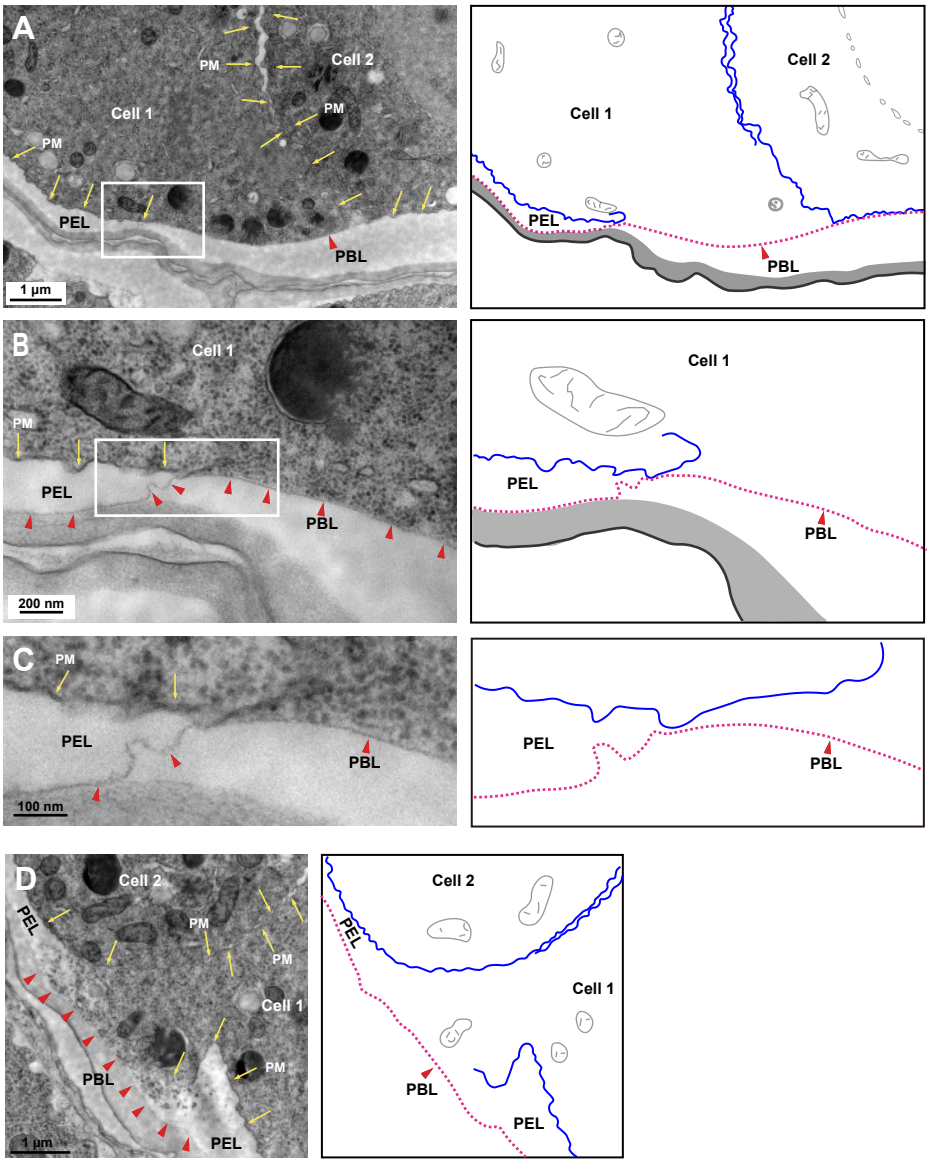
A
PM
Cell 2
Cell 1
PM
PM
PEL
PBL
1 µm
Cell 2
Cell 1
PEL
PBL
B
Cell 1
PM
PEL
PBL
200 nm
Cell 1
PEL
PBL
C
PM
PEL
PBL
100 nm
PEL
PBL
D
Cell 2
PEL
PM
PM
Cell 1
PM
PBL
PEL
1 µm
Cell 2
PEL
Cell 1
PBL
PEL

Sup Figure 1

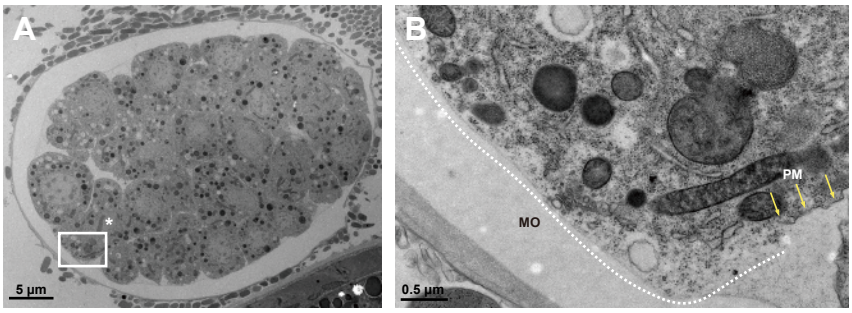

Sup Figure 2

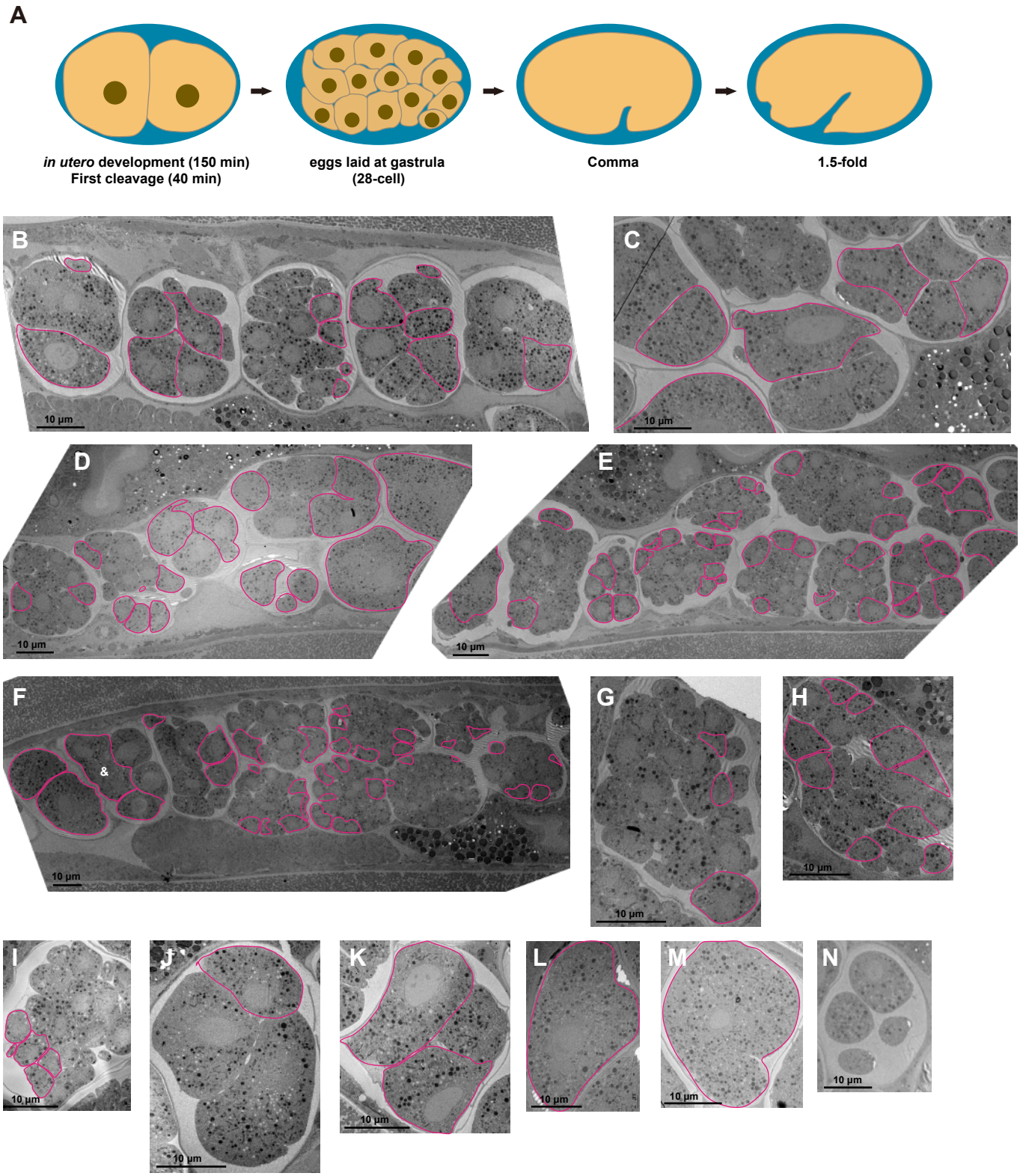
A
in utero development (150 min)
First cleavage (40 min)
eggs laid at gastrula
(28-cell)
Comma
1.5-fold
B
C
D
E
F
&
G
H
I
J
K
L
M
N
10 µm

Sup Figure 3

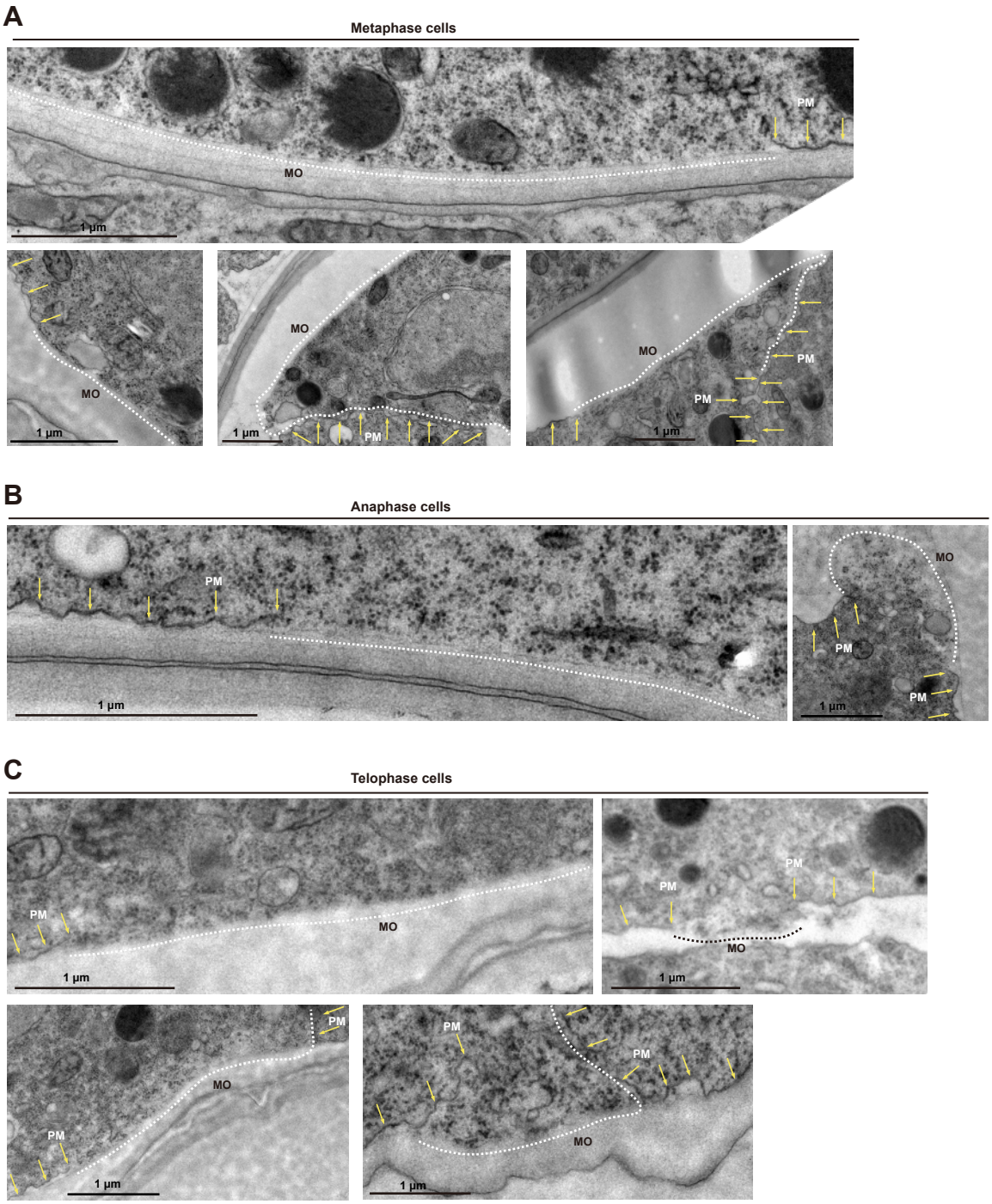
A
Metaphase cells
PM
MO
1 µm
MO
1 µm
MO
1 µm
PM
MO
PM
PM
1 µm
B
Anaphase cells
PM
1 µm
MO
PM
PM
1 µm
C
Telophase cells
PM
MO
1 µm
PM
PM
MO
1 µm
PM
MO
PM
1 µm
PM
PM
MO
1 µm